Double-Conversion, Noise-Cancelling Receivers Using Modulated LNTAs and Double-Layer Passive Mixers for Concurrent Signal Reception With Tuned RF Interface

Guoxiang Han[®], Member, IEEE, and Peter R. Kinget[®], Fellow, IEEE

Abstract—A double-conversion, noise-cancelling receiver architecture is presented that consists of a double-layer mixer-first branch and two quadrature-modulated LNTA branches. The two layers of passive mixing in the mixer-first branch up-convert the low-pass, baseband impedance and create concurrent, narrowband impedance matching at $(F_{LO} \pm F_{IF})$, as well as concurrently receive signals around these two RF carriers while rejecting spurious responses without using any IF filters. To improve the noise performance, quadrature-modulated LNTA branches are incorporated to allow frequency-translational, noise cancellation for better receiver sensitivity. Double conversion is achieved in the LNTA branches by periodically varying the LNTA transconductance and current-mode, passive mixing. A generalized, linear time-varying (LTV) analysis of the receiver is presented and verified with behavioral-model simulation results.

Index Terms—Concurrent signal reception, harmonic rejection (HR), mixer-first, multi-carrier, noise cancellation, RF, wideband.

I. INTRODUCTION

RALY receivers for GPS and GSM terminals usually adopted multiple frequency conversions with filtering before each conversion stage [1]. As CMOS processes advanced, direct-conversion receivers helped reduce cost and system complexity and are widely used. The frequency-translational, noise-cancelling (FTNC) receiver [2] is a direct-conversion receiver architecture; its mixer-first branch provides tuned RF input impedance matching by translating the low-pass, baseband impedance to its LO frequency. Its auxiliary, low-noise transconductance-amplifier (LNTA) branch measures the up-converted noise from the mixer-first branch at RF input; the baseband outputs of these two signal branches are combined to achieve noise cancellation for better receiver sensitivity.

Nowadays, with the exponentially increasing demands on wireless throughput, the mainstream communication standards [3] require that handset receivers support carrier aggregation (CA) to receive multiple RF carriers concurrently from either the same band (*intra-band*) or different bands (*inter-band*). Since the RF input impedance of the FTNC

Manuscript received December 24, 2020; revised March 23, 2021 and May 23, 2021; accepted June 2, 2021. Date of publication June 14, 2021; date of current version August 10, 2021. This work was supported in part by NSF under Award 1733857. This article was recommended by Associate Editor D. Zhao. (Corresponding authors: Guoxiang Han; Peter R. Kinget.)

The authors are with the Department of Electrical Engineering, Columbia University, New York, NY 10027 USA (e-mail: gh2423@columbia.edu; kinget@ee.columbia.edu).

Color versions of one or more figures in this article are available at https://doi.org/10.1109/TCSI.2021.3086708.

Digital Object Identifier 10.1109/TCSI.2021.3086708

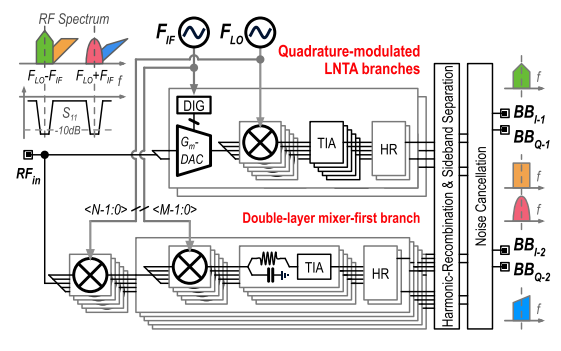


Fig. 1. Simplified diagram of the double-conversion, noise-cancelling receiver, featuring concurrent tuned matching, concurrent reception, noise cancellation, and rejection of spurious responses.

receiver is 50Ω around its LO frequency and low elsewhere, multiple FTNC receivers operating with different LOs cannot be directly connected in parallel at the RF input for inter-band CA. Instead, external passive filter networks in the front-end module are required to isolate receivers when put in parallel for inter-band CA. Commercial solutions use this strategy to split the inter-band RF carriers to different signal chains and down-convert them to baseband, separately. However, the filter networks are typically not tunable, leading to highly complex configurations [4], especially when CA across a flexible set of inter-band RF carriers is desired.

Recent research explored different techniques to enable this desired feature. The frequency-translational, quadrature-hybrid receiver [5] combines the concepts of balanced amplifiers with current-mode receivers for flexible, inter-band reception. Thanks to its balanced structure, the termination noise gets cancelled for good noise performance. However, its broadband input interface provides no RF selectivity, resulting in limited out-of-band linearity. The harmonic-selective FTNC receiver [6] combines the FTNC receiver concept with over-sampling mixers and applies 32-phase non-overlapping clocks. It can receive inter-band carriers but only if they are harmonically allocated. To receive arbitrarily-allocated carriers, the gain-boosted N-path-filter receiver [7] uses two bandstop, N-path filters as the feedback network to a broadband amplifier, realizing tuned impedance matching at two distinct bands simultaneously, but does not allow for noise cancellation, affecting its noise performance. The active feedback further limits both in-band and out-of-band linearity. The multi-branch, modulated-mixer-clock receiver [8] explores clock modulation for tuned matching at two arbitrarilyallocated carriers and also noise cancellation. However,

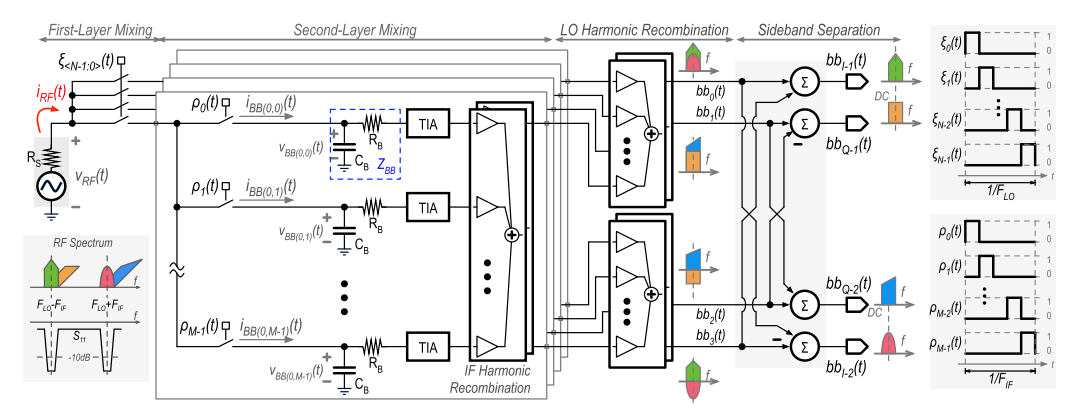


Fig. 2. Block diagram of the double-layer mixer-first branch using two layers of passive mixing at F_{LO} and F_{IF} and providing narrow-band impedance matching at $(F_{LO} \pm F_{IF})$ while concurrently receiving the I/Q information from these two RF carriers.

the spurious responses due to its clock modulation are not suppressed.

In this article, we present the analysis of a doubleconversion, noise-cancelling receiver architecture (Fig. 1), featuring the concurrent reception from two inter-band carriers, a tuned RF interface, noise cancellation, and the rejection of spurious responses. We first study the double-conversion operation and the unique properties of multi-phase, double-layer passive mixers [9] (also referred to as N-path filters) in Section II. As shown in Fig. 1, the first-layer passive mixers are connected to the RF input and clocked at F_{LO} . The second-layer mixers are clocked at F_{IF} and loaded with lowpass, baseband impedances. This structure up-converts the baseband impedance first to F_{IF} and then to $(F_{LO} \pm F_{IF})$, resulting in tuned, high-Q bandpass RF impedance matching in two frequency bands and low input impedance elsewhere, and eliminating the use of external passive filter networks. Meanwhile, it down-converts the RF carriers at these two frequencies and serves as a mixer-first receiver for concurrent signal reception, while rejecting harmonic responses without needing IF filters.

Next, in Section III, we analyze the operation and properties of quadrature-modulated LNTAs followed by multiphase, current-mode passive mixers clocked at F_{LO} ; the LNTA transconductance is modulated sinusoidally at F_{IF} using direct digital synthesis [10]. This circuit also performs concurrent signal reception from ($F_{LO} \pm F_{IF}$), while rejecting harmonic responses without using IF filters. However, it does not provide any impedance matching at the RF input.

Then, we combine these two types of signal branches to form a double-conversion, noise-cancelling receiver for better sensitivity. As described in Section IV, by combining the branches' outputs with appropriate gain coefficients, the noise of mixer switch resistors, baseband termination resistors and op-amps from the mixer-first branch is cancelled, while the concurrent tuned RF interface and dual-band concurrent reception is preserved. We provide a generalized LTV analysis of the various structures and study their RF input impedance, conversion gain and noise performance, as well as sideband rejection and harmonic folding and rejection. Simulation results are presented that confirm the analytical results.

II. MIXER-FIRST RECEIVER BRANCH USING DOUBLE-LAYER PASSIVE MIXERS

A. Principle of Operation

The double-layer mixer-first branch (MFB) in Fig. 2 creates an RF interface with tuned impedance matching at $(F_{LO} \pm F_{IF})$

simultaneously. Each second-layer mixing circuit is composed of M-phase passive mixers clocked at F_{IF} with M-phase 1/M-duty-cycle, non-overlapping clocks, $\rho_0(t)$ to $\rho_{M-1}(t)$, termination resistors R_B and capacitors C_B , and M baseband transimpedance amplifiers (TIAs), followed by two F_{IF} harmonic recombining circuits. They sum the weighted TIA output voltages to reject responses at higher-order F_{IF} harmonics [2]. Each set of second-layer mixers has a tuned input impedance centered at F_{IF} . By using N second-layer mixers as the termination for the first-layer, N-phase passive mixers clocked at F_{LO} with N-phase 1/N-duty-cycle, non-overlapping clocks, $\xi_0(t)$ to $\xi_{N-1}(t)$, the tuned RF interface is translated to $(F_{LO} \pm F_{IF})$ simultaneously (Fig. 2). In practice, to simplify clock generation, N, M are integers greater than two and are typically powers of two (e.g., 8, 16, etc.)

The signal carriers around $(F_{LO} \pm F_{IF})$ in the RF input signal, $v_{RF}(t)$, are first down-converted to F_{IF} and then to baseband. The 2N baseband outputs are harmonically combined into four linearly-independent, baseband outputs, $bb_0(t)$ to $bb_3(t)$, while rejecting input signals around higher-order F_{LO} harmonics [2]. The I/Q components from each signal carrier, $bb_{I/Q-1}(t)$ and $bb_{I/Q-2}(t)$, can be separated using simple addition and subtraction circuits as shown in Fig. 2. For example, the I-phase component from the lower RF carrier at $(F_{LO} - F_{IF})$ can be extracted by adding the signals $bb_0(t)$ and $bb_3(t)$, whereas subtracting these two signals gives the I-phase component from the higher RF carrier.

A unique feature of the double-layer mixer branch is that it uses multi-phase F_{LO} clocks, such that the I/Q components of two RF carriers can be obtained from the linearly independent baseband outputs, $bb_0(t)$ to $bb_3(t)$, without any IF filtering. In traditional double-conversion receivers with IF filtering, only two phases for the F_{LO} clocks are used, providing insufficient information to separate the different input carriers, so that only a single RF carrier is received.

B. RF Input Interface

The double-layer mixer-first branch can be treated as an *N*-path filter, terminated with *M*-path filters that are loaded with low-pass, baseband impedances. The double-layer mixers can be implemented as both single-ended, as a single-ended-differential combination, or as both differential. We first analyze the fully single-ended realization in Fig. 2 using the frequency-domain analysis technique from [11] and then give expressions for the other two realizations with detailed derivations available in [12]. Note that this technique does not

model the power loss due to harmonic re-upconversion by the passive mixers (i.e., R_{sh} in [13]), which results in slight errors between analytical and simulated results for conversion gain and noise performance. However, it allows us to understand the frequency translations of the impedances. Moreover, as the number of F_{LO} and F_{IF} clock phases increases (e.g., when $N, M \geq 8$), the power loss becomes quickly negligible [14], as is the case for practical implementations.

We define $Z_{BB}(\omega)$ (Fig. 2) as the low-pass, baseband impedance, and $z_{BB}(t)$ as its corresponding impulse response. Here we assume the TIAs provide good virtual grounds within the desired frequency band, such that $Z_{BB}(\omega)$ is determined by R_B and C_B . Given the use of non-overlapping clocks, at any given moment, the RF current $i_{RF}(t)$ flows into only one baseband path. The current for the $(x, y)^{th}$ baseband path is:

$$i_{BB(x,y)}(t) = \left[\xi_x(t)\rho_y(t)\right] \cdot i_{RF}(t). \tag{1}$$

This current then flows into $z_{BB}(t)$ and produces the voltage:

$$v_{BB(x,y)}(t) = \left\{ \left[\xi_x(t) \rho_y(t) \right] \cdot i_{RF}(t) \right\} * z_{BB}(t) \tag{2}$$

where * denotes convolution. To find the voltage at the RF side of the switches, $v_{RF}(t)$, we observe that, at any given moment, it is equal to the voltage across the appropriate $(x, y)^{th}$ baseband impedance, plus the ohmic drop across two mixer switches in series:

$$v_{RF}(t) = 2R_{SW} \cdot i_{RF}(t) + \sum_{x=0}^{N-1} \sum_{y=0}^{M-1} \left[\xi_x(t) \rho_y(t) \right]$$

$$\cdot \langle \left\{ \left[\xi_x(t) \rho_y(t) \right] \cdot i_{RF}(t) \right\} * z_{BB}(t) \rangle$$
(3)

where R_{SW} is the switch resistance, which we assumed equal for both layers. The Fourier series of $\xi_x(t)$ is:

$$\xi_x(t) = \sum_{k=-\infty}^{+\infty} \alpha_k \exp(-jxk\frac{2\pi}{N}) \exp(jk\omega_{LO}t)$$
 (4)

where $\alpha_k = (1/N) \operatorname{sinc}(k\pi/N) \exp(-jk\pi/N)$ and the Fourier series of $\rho_v(t)$ is:

$$\rho_{y}(t) = \sum_{l=-\infty}^{+\infty} \beta_{l} \exp(-jyl\frac{2\pi}{M}) \exp(jl\omega_{IF}t)$$
 (5)

where $\beta_l = (1/M) \operatorname{sinc}(l\pi/M) \exp(-jl\pi/M)$. Using properties of the Fourier series, we calculate the summation term in (3):

$$\mathcal{F}\langle \left[\xi_{x}(t)\rho_{y}(t) \right] \cdot \left\{ \left[\xi_{x}(t)\rho_{y}(t) \right] \cdot i_{RF}(t) * z_{BB}(t) \right\} \rangle$$

$$= \sum_{k=-\infty}^{+\infty} \sum_{l=-\infty}^{+\infty} \sum_{p=-\infty}^{+\infty} \sum_{q=-\infty}^{+\infty} \alpha_{k}\beta_{l}\alpha_{p}\beta_{q}$$

$$\cdot \exp \left[-jx(k+p)\frac{2\pi}{N} \right] \exp \left[-jy(l+q)\frac{2\pi}{M} \right]$$

$$\cdot I_{RF} \left[\omega - (k+p)\omega_{LO} - (l+q)\omega_{IF} \right]$$

$$\cdot Z_{BB} \left[\omega - (p\omega_{LO} + q\omega_{IF}) \right]. \tag{6}$$

Now, the Fourier transform of $v_{RF}(t)$ is obtained as:

$$V_{RF}(\omega) = 2R_{SW} \cdot I_{RF}(\omega) + NM \cdot \sum_{k=-\infty}^{+\infty} \sum_{l=-\infty}^{+\infty} \sum_{p=-\infty}^{+\infty} \sum_{q=-\infty}^{+\infty} \alpha_k \beta_l \alpha_p \beta_q$$

$$I_{RF} \left[\omega - (k+p)\omega_{LO} - (l+q)\omega_{IF} \right]$$

$$\cdot Z_{BB} \left[\omega - (p\omega_{LO} + q\omega_{IF}) \right]$$
 (7)

where $(k+p)=k_1$ N, $(l+q)=k_2$ M, and $k_1,k_2\in\mathbb{Z}$. For a sinusoidal, incident RF current at $[\Delta\omega+(\omega_{LO}-\omega_{IF})]$, where $\Delta\omega$ is a small frequency offset, the voltage at RF input, $V_{RF}(\omega)$, will have a main component at $[\Delta\omega+(\omega_{LO}-\omega_{IF})]$ but also smaller components at $[\Delta\omega+(k_1\ N+1)\omega_{LO}+(k_2\ M-1)\omega_{IF}]$. The impedance translation coefficients for these components are significantly smaller than for the main component [11]. Therefore, we can ignore these components except for (k+p)=0 and (l+q)=0; $V_{RF}(\omega)$ becomes a function of only $I_{RF}(\omega)$. The RF input impedance can be derived as:

$$Z_{in}(\omega) \equiv \frac{V_{RF}(\omega)}{I_{RF}(\omega)} = 2R_{SW} + NM$$

$$\cdot \sum_{p=-\infty}^{+\infty} \sum_{q=-\infty}^{+\infty} |\alpha_p|^2 |\beta_q|^2 \cdot Z_{BB}[\omega - (p\omega_{LO} + q\omega_{IF})].$$
(8)

Fig. 3 shows the analytical and simulated S_{11} profiles using N=M=8. The S_{11} profile has the desired impedance matching at $(F_{LO}\pm F_{IF})$ but also has spurious matching at $(pF_{LO}+qF_{IF})$ where $p,q\in\mathbb{Z}$. To achieve better S_{11} profiles with less spurious matching, we observe that the first-layer passive mixers produce differential outputs. The second-layer passive mixers can be realized in a differential manner. The RF input impedance is now¹:

$$Z'_{in}(\omega) = 2 R_{SW} + \frac{NM}{2} \cdot \sum_{p=-\infty}^{+\infty} \sum_{q=-\infty}^{+\infty} |\alpha_p|^2 |\beta_q|^2 \cdot \left\{ 1 + \exp\left[-j(p+q)\pi\right] \right\}^2 \cdot Z_{BB}[\omega - (p\omega_{LO} + q\omega_{IF})].$$
(9)

Fig. 3 shows the analytical and simulated S_{11} profiles. The calculated and simulated, RF matching bandwidths are 34.8MHz and 36.3MHz, respectively. The number of frequencies where spurious matching occurs reduces significantly. However, undesired impedance matching still happens at $(pF_{LO}+qF_{IF})$ where (p+q) is even. A differential realization for both the first- and the second-layer mixers further improves the S_{11} profiles; the unwanted matching gets suppressed for even p and q. The differential RF input impedance is:

$$Z_{in}''(\omega) = 4 R_{SW} + \frac{NM}{2} \cdot \sum_{p=-\infty}^{+\infty} \sum_{q=-\infty}^{+\infty} |2\alpha_p|^2 |2\beta_q|^2 \cdot Z_{BB}[\omega - (p\omega_{LO} + q\omega_{IF})]$$

$$(10)$$

where p,q are both odd integers. As shown in Fig. 3, impedance matching now occurs for $(F_{LO} \pm F_{IF})$ as desired with a few sets of undesired responses [e.g., $(F_{LO} \pm 3 F_{IF})$] creating significant matching within the practical bandwidth, whereas a low input impedance exists for all

¹To distinguish different expressions for different realizations (e.g., for input impedance, gain, and noise), we use $(\cdot)'$ for the single-ended-differential realization and $(\cdot)''$ for the fully differential realization, whereas the expressions without these symbols are for the fully single-ended realization.

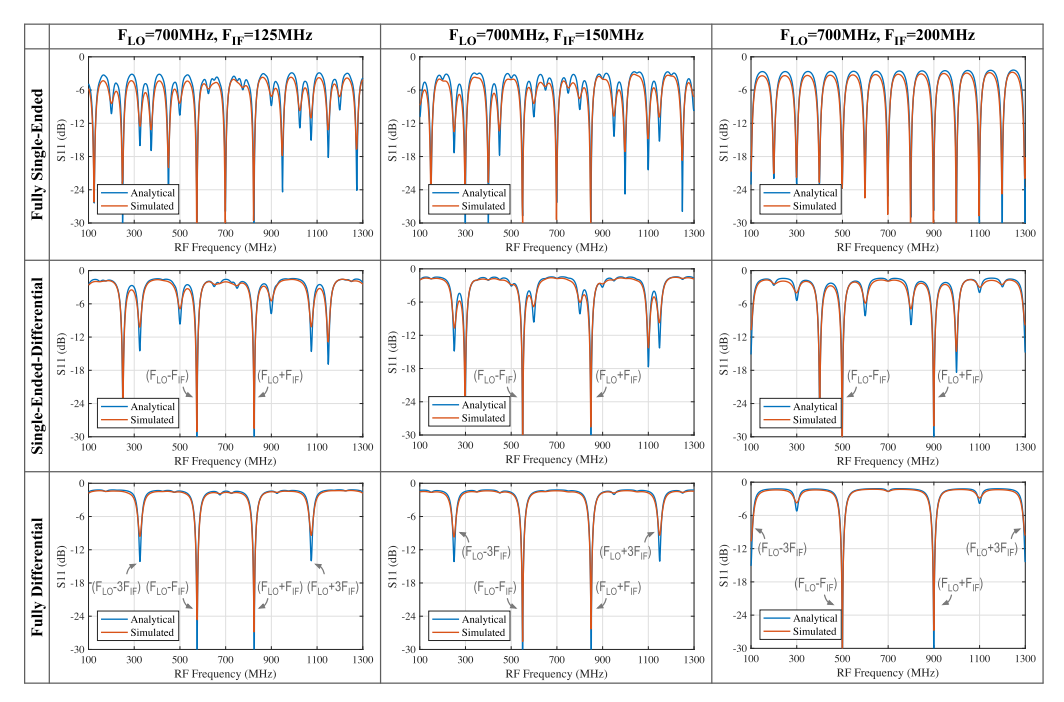


Fig. 3. Comparison of analytical and simulated S_{11} profiles for different mixer-first branch realizations for $F_{LO}=700 {\rm MHz}$ and $R_{SW}=1.5\Omega$ but different F_{IF} clock rates. For the fully single-ended realization, $R_S=50\Omega$, $R_B=3.34 {\rm k}\Omega$ and $C_B=5 {\rm p}{\rm F}$; for the single-ended-differential realization, $R_S=50\Omega$, $R_B=1.67 {\rm k}\Omega$ and $C_B=10 {\rm p}{\rm F}$; for the fully differential realization, $R_S=100\Omega$, $R_B=0.83 {\rm k}\Omega$ and $C_B=20 {\rm p}{\rm F}$.

other frequencies.² The calculated and simulated, RF matching bandwidths are 36.5MHz and 38.3MHz, respectively. Therefore, for receiver systems allowing the use of RF input baluns, it is desirable to use the fully-differential realization for its good matching profiles. For receiver systems that do not allow the use of baluns due to the limited form factor or system complexity,³ it is recommended to use the single-ended-differential realization.

a) Trade-off between 'large' and 'small' mixer-switch sizing: In a 'large' design, the mixers are sized for small R_{SW} . Accordingly, for a given bandwidth, the resistors R_B can be sized larger, and the capacitors C_B can be smaller. Small R_{SW} results in a low out-of-band impedance and thus good out-of-band signal reflection; such up-front filtering profile protects the LNTA branches from strong out-of-band blocking signals. However, this choice faces design challenges, such as larger parasitic switch capacitance and high switch-clock dynamic power. Using processes with reduced parasitics (e.g., SOI) can significantly mitigate those challenges. In a 'small'switch mixer design (i.e., with larger R_{SW}), these challenges are mitigated to some extent. However, to maintain the impedance matching with the same bandwidth, R_B needs to be small, which requires large C_B . Although modern CMOS processes have been scaled towards finer transistor feature lengths, the capacitance density has not scaled as much, and capacitors can require a lot of area.

C. Conversion Gain

As discussed previously, for a single-ended RF input, the single-ended-differential realization has a better matching profile, compared to its fully single-ended counterpart. Therefore, in the following parts, we will study this realization in Fig. 4; the detailed derivations of the fully-differential realization are available in [12]. The conversion gain of this realization is:

$$CG'_{MFB} \equiv \frac{V_{BB,I-1}}{V_{RF}} = \frac{R_{F,MFB}}{2R_{SW} + 2\eta R_B} \cdot G_{MX,LO}G_{MX,IF} \cdot \frac{NM}{2}$$
$$= \frac{1}{2} \cdot \frac{R_{F,MFB}}{2R_{SW} + 2\eta R_B} \cdot \operatorname{sinc}(\pi/N) \cdot \operatorname{sinc}(\pi/M) \quad (11)$$

where $R_{F,MFB}$ is the TIA feedback resistance; $G_{MX,LO} = (1/N)\mathrm{sinc}(\pi/N)$ and $G_{MX,IF} = (1/M)\mathrm{sinc}(\pi/M)$ are the current conversion gains of the passive mixers driven by F_{LO} and F_{IF} clocks [16], respectively; η is the impedance translation coefficient and can be derived from (8) as:

$$\eta = \frac{\operatorname{sinc}^{2}(\pi/N)}{N} \cdot \frac{\operatorname{sinc}^{2}(\pi/M)}{M}.$$
 (12)

We intentionally leave R_B as a design parameter, such that (11) is a generalized gain expression. If impedance matching to the antenna source resistance, R_S , is desired:

$$R_B' = \frac{R_S - 2 \ R_{SW}}{2\eta}. (13)$$

For N=M=8, $R_S=50\Omega$, and $R_{SW}=10\Omega$, R_B is $1.06k\Omega$ for input matching. As N,M increases, both sinc factors approach to unity, leading to better noise and harmonic performance.

D. Noise

For well-designed receivers, R_S , R_{SW} , R_B , and the baseband op-amps in the TIAs are the dominant sources of noise,

²This impedance up-conversion from baseband to intermodulation products of higher-order F_{LO} and F_{IF} clock harmonics stems from passive mixer transparency [11], [15]. It cannot be suppressed with larger numbers of clock phases (i.e., larger N, M).

³The handset receivers for GSM and CDMA mostly use differential RF inputs to make use of common-mode rejection and to leverage the shrinking voltage headroom. However, for LTE and NR, the differential interface gives ways to its single-ended counterpart due to the exploding number of supported bands (especially for CA), the limited number of package pins, and the cost for differential matching networks [4].

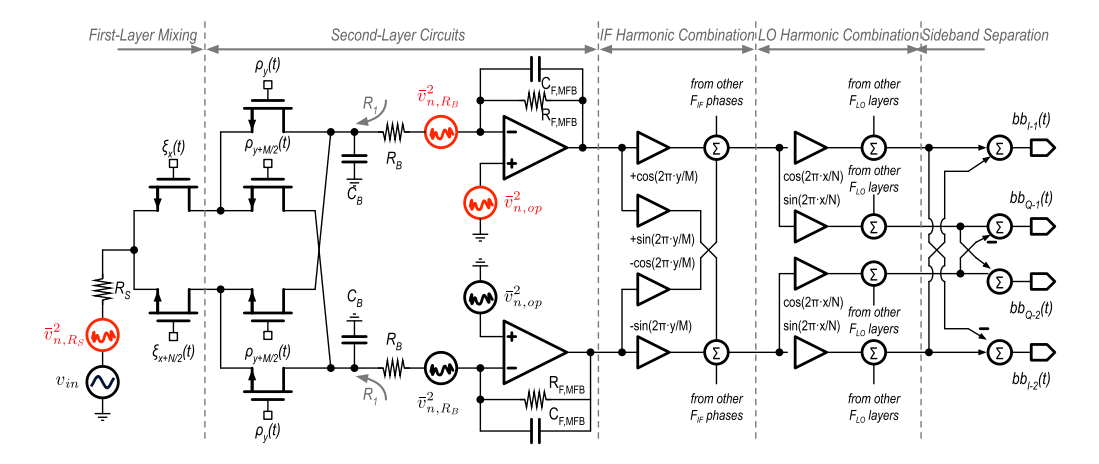


Fig. 4. Schematic of the $(x, y)^{th}$ path of a singled-ended-differential realization of the double-layer mixer-first branch.

while $R_{F,MFB}$ does not contribute significant noise [17]. The baseband TIA typically offers a good virtual ground at the baseband frequencies of interest, which simplifies the analysis (14), as shown at the bottom of the page.

1) Noise From R_S and R_{SW} : These noise sources have a transfer function to the branch output similar to that of the desired signals, except that noise folding needs to be accounted for. The output noise contribution due to R_S is:

$$\frac{\overline{v_{no,R_S}^2}}{\Delta f} = \frac{\overline{v_{n,R_S}^2}}{\Delta f} \cdot \left(\frac{2R_{SW} + 2\eta R_B}{R_S + 2R_{SW} + 2\eta R_B} \cdot CG'_{MFB,N-M}\right)^2 \cdot \frac{2}{\operatorname{sinc}^2(\pi/M) \cdot \operatorname{sinc}^2(\pi/N)}$$
(15)

where $\overline{v_{n,R_S}^2}/\Delta f = 4kTR_S$ [18], and the factor in the brackets accounts for the voltage division between R_S and the in-band input resistance $R_{in}=2$ $R_{SW}+2\eta R_B$; in the last factor, the numerator of '2' accounts for the noise down-conversion from both lower and upper sidebands around the RF carrier, whereas the sinc factors in the denominator model the noise folding [19] from higher-order intermodulation products of the F_{LO} and F_{IF} clocks.

2) Noise From R_B : Each path has a termination resistor. Given the non-overlapping nature of the F_{LO} and F_{IF} clocks, the noise from one signal path does not propagate to the other paths, so they are orthogonal in time. Since the resistors are physically different, their noise is uncorrelated. Therefore, we can study the noise from one path and then sum up the noise powers for all paths with corresponding weights for harmonic recombination and sideband separation.

Fig. 4 shows the simplified schematic of the $(x, y)^{th}$ path; the noise of R_B can be modelled with a series voltage source, which only conducts noise current when $\xi_x(t) \cdot \rho_y(t)$ is high or when $\xi_{x+N/2}(t) \cdot \rho_{y+M/2}(t)$ is high. The average resistance

looking back into the mixer network at baseband, R_1 , is then⁴:

$$R_1 = \frac{NM}{2} \cdot (R_S + 2 \ R_{SW}). \tag{16}$$

Thus, the output noise due to R_B in the $(x, y)^{th}$ path is:

$$\frac{\overline{v_{no,R_B(x,y)}^2}}{\Delta f} = \frac{\overline{v_{n,R_B}^2}}{\Delta f} \cdot \left[\frac{R_{F,MFB}}{R_B + R_1} \cdot \cos\left(\frac{2\pi}{N}x - \frac{2\pi}{M}y\right) \right]^2$$
(17)

where $\overline{v_{n,R_B}^2}/\Delta f = 4kTR_B$ [18], and the cos factor is the coefficient due to harmonic recombination and sideband separation. Utilizing the orthogonal and uncorrelated properties, the output noise due to all R_B 's is then:

$$\frac{\overline{v_{no,R_B}^2}}{\Delta f} = \sum_{x=0}^{N/2-1} \sum_{y=0}^{M-1} \frac{\overline{v_{no,R_B(x,y)}^2}}{\Delta f} \\
= \frac{\overline{v_{n,R_B}^2}}{\Delta f} \cdot \frac{NM}{4} \cdot \left(\frac{R_{F,MFB}}{R_B + R_1}\right)^2.$$
(18)

3) Noise From Baseband Op-Amps: We model the noise of baseband op-amps in the TIAs as noise voltage sources at their non-inverting input (Fig. 4), and the analysis is similar to that for R_B . The output noise due to all the baseband op-amps is:

$$\frac{\overline{v_{no,op}^2}}{\Delta f} = \frac{\overline{v_{n,op}^2}}{\Delta f} \cdot \frac{NM}{4} \cdot \left(1 + \frac{R_{F,MFB}}{R_B + R_1}\right)^2 \tag{19}$$

where $\overline{v_{n,op}^2}/\Delta f = 4kT\gamma/G_{m,op}$ [18].

⁴Since $\xi_X(t)$ and $\rho_Y(t)$ have duty cycles of 1/N and 1/M, respectively, $\xi_X(t) \cdot \rho_Y(t)$ has a duty cycle of 1/(NM) for the period whose value is the inverse of the least common multiple (LCM) of the F_{LO} and the F_{IF} clock frequencies. Similarly, $\xi_{X+N/2}(t) \cdot \rho_{Y+M/2}(t)$ also has a duty cycle of 1/(NM) over the same period. Within the desired, baseband channel frequencies, C_B is open and R_1 becomes $(NM/2) \cdot (R_S+2 R_{SW})$. At higher frequencies, C_B can be considered as a short circuit to ground.

$$F'_{MFB,N-M} \approx \frac{1}{\operatorname{sinc}^{2}(\pi/N) \cdot \operatorname{sinc}^{2}(\pi/M)} \cdot \left\{ 1 + \frac{2R_{SW}}{R_{S}} + \frac{R_{B}}{R_{S}} \cdot \frac{2}{NM} + \frac{\gamma}{G_{m,op}R_{S}} \cdot \frac{2}{NM} \cdot \left[1 + \frac{(R_{S} + 2R_{SW}) \cdot (NM/2) + R_{B}}{R_{F,MFB}} \right]^{2} \right\}$$
(14)

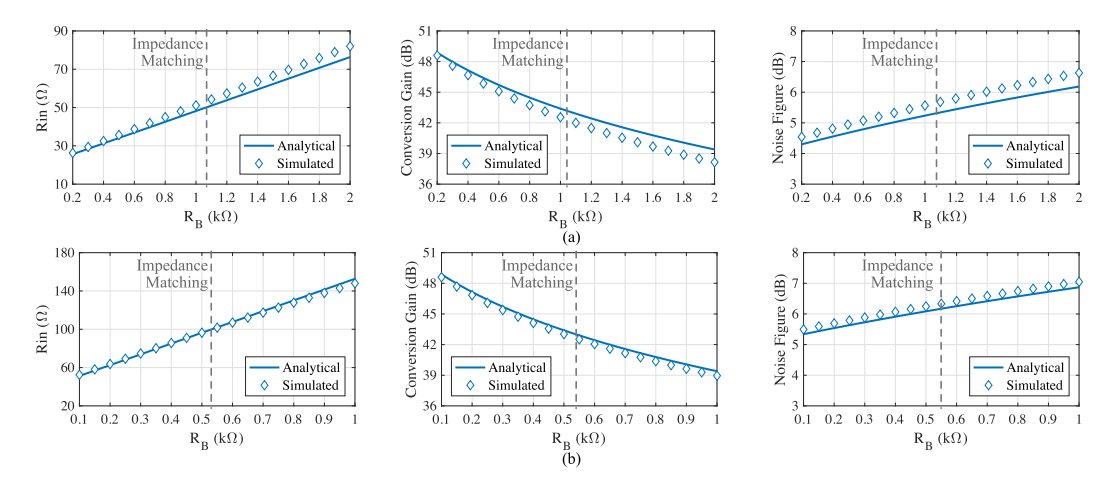


Fig. 5. Analytical and simulated in-band input resistance, conversion gain, and NF versus R_B for N=M=8, $F_{LO}=700 \text{MHz}$, $F_{IF}=150 \text{MHz}$, $R_{SW}=10\Omega$, $R_{F,MFB}=15 \text{k}\Omega$, $G_{m,op}=625 \text{uS}$, and $\gamma=2/3$: (a) Single-ended-differential realization with $R_S=50\Omega$; (b) Fully differential realization with $R_S=100\Omega$.

4) The Noise Factor: of the mixer-first branch⁵ in a single-ended-differential realization, $F'_{MFB,N-M}$, can be derived by comparing the total output noise with the output noise due to R_S in (14). The sinc factors approach unity when the numbers of clock phases increase, and when N=M=8, the noise factor becomes:

$$F'_{MFB,8-8} \approx \frac{1}{\sin^{4}(\pi/8)} \cdot \left\{ 1 + \frac{2R_{SW}}{R_{S}} + \frac{R_{B}}{32 \cdot R_{S}} + \frac{\gamma}{32 \cdot G_{m,op}R_{S}} \cdot \left[1 + \frac{32 \cdot (R_{S} + 2R_{SW}) + R_{B}}{R_{F,MFB}} \right]^{2} \right\}.$$
(20)

Implications of these expressions will be discussed and verified with simulation results in Section II-F.

E. Harmonic Folding

Because of the time-varying nature of the passive mixers, mixer-first designs inevitably face challenges of harmonic folding, meaning that undesired signals at clock harmonics can fold to the desired signal band. For standard, single-layer mixer-first branches using N-phase clocks at F_{LO} [14], [20], the harmonic folding rejection ratio (HFRR) is the ratio of the gain of the wanted RF signals to the gain of the unwanted RF signals that fold back on top of the desired signal band [21]:

$$HFRR_n = \left| \frac{\operatorname{sinc}(\pi/N)}{\operatorname{sinc}(n\pi/N)} \right| \tag{21}$$

where $n = kN \pm 1$ and $k \in \mathbb{Z}$. For the double-layer mixer-first branch, to the first order, its HFRR can be obtained by multiplying two HFRR expressions:

$$HFRR_{n,m} = \left| \frac{\operatorname{sinc}(\pi/N)}{\operatorname{sinc}(n\pi/N)} \cdot \frac{\operatorname{sinc}(\pi/M)}{\operatorname{sinc}(m\pi/M)} \right|$$
 (22)

where $n = k_1$ $N \pm 1$, $m = k_2$ $M \pm 1$, and $k_1, k_2 \in \mathbb{Z}$. Increasing the number of clock phases, especially for the F_{IF} clocks, mitigates harmonic folding. For example, when N = M = 8, $F_{LO} = 700 \text{MHz}$ and $F_{IF} = 150 \text{MHz}$,

the response at $(F_{LO}-9\ F_{IF})$ or 650MHz will be folded back to the lower-carrier baseband output, whereas the response at $(F_{LO}-7\ F_{IF})$ or 350MHz will be folded back to the higher-carrier baseband output. Using a larger M (e.g., 16 and beyond) eliminates these two responses but at the cost of reducing the maximum RF operating frequency and increasing the dynamic switch power due to the parasitics from the switching devices [20].

F. Simulations and Design Considerations

Fig. 5 shows the analytical and simulated in-band input resistance R_{in} , conversion gain, and noise figure (NF) versus R_B . The simulations use periodic steady-state and periodic noise analyses with a shooting engine [22] for noise analysis. Results agree well when R_B is small. As R_B increases, the effect of R_{sh} (see Section II-B) becomes more pronounced, and the analytical results deviate from the simulated values. In practice, R_B is sized for impedance matching (see Section II-C), whose values are indicated on Fig. 5.

1) Comparison to Single-Layer Branches: To concurrently receive two inter-band RF carriers with single-layer mixer-first branches [17], an external passive filter network is needed for isolation (see Section I), which requires extra board space and introduces additional signal loss. For now, we assume that the filter network has zero signal loss and compare this case with the proposed case in term of power consumption for baseband circuits and clock buffering circuits.

a) Baseband consumption: The noise factor of a single-ended, single-layer mixer-first branch [12] is:

$$\widetilde{F}_{MFB,N} = \frac{1}{\operatorname{sinc}^{2}(\pi/N)} \cdot \left\{ 1 + \frac{R_{SW}}{R_{S}} + \frac{R_{B}}{R_{S}} \cdot \frac{1}{N} + \frac{\gamma}{\widetilde{G}_{m,op}R_{S}} \cdot \frac{1}{N} \cdot \left[1 + \frac{N \cdot (R_{S} + R_{SW}) + R_{B}}{R_{F,MFB}} \right]^{2} \right\}$$
(23)

where $\widetilde{G}_{m,op}$ is used to model the noise of each baseband op-amp; there are 2N op-amps on chip, whereas the proposed approach in a single-ended-differential realization uses (NM)/2 op-amps. Assuming the same transistor biasing condition and the same power consumption, we have:

$$2N \cdot \widetilde{G}_{m,op} = \frac{NM}{2} \cdot G_{m,op}. \tag{24}$$

⁵We use the double-sideband noise factor here since its value is the same as the single-sideband noise factor after image rejection is performed. The image rejection is typically done in the digital domain using the down-converted I/Q baseband signals.

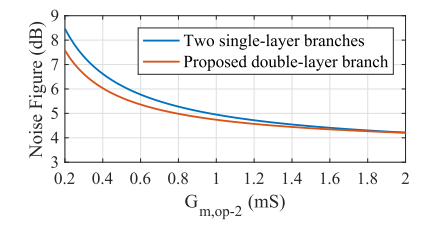


Fig. 6. Noise performance comparison of the single-layer case with the proposed case using the same design parameters as in Fig. 5. For the single-layer case, R_B is $0.34 \mathrm{k}\Omega$ for impedance matching; for the double-layer case, R_B is $1.06 \mathrm{k}\Omega$.

Elaborating (14), (23) and (24), Fig. 6 plots the calculated NFs of both cases as a function of $G_{m,op}$, assuming the impedance matching condition. For the same current consumption, the proposed case has a smaller NF compared to the single-layer case, or for the same noise performance, the proposed case has a smaller baseband current consumption.

b) Dynamic clock consumption: The mixer switches in this comparison are assumed to have the same size, yielding the same gate capacitance C_G . With a fan-out-of-four (FO-4) driving scheme, the dynamic buffering power of the first case, where the two branches are driven by N-phase, non-overlapping clocks at $(F_{LO} - F_{IF})$ and $(F_{LO} + F_{IF})$, is:

$$\widetilde{P}_{CLK} = \frac{1}{2} \cdot \frac{4}{3} \cdot NC_G V_{DD}^2 \cdot [(F_{LO} - F_{IF}) + (F_{LO} + F_{IF})]$$

$$= C_G V_{DD}^2 \cdot \frac{4}{3} N \cdot F_{LO}$$
(25)

where two sets of *N*-phase mixers are used for the first case. The dynamic buffering power of the proposed case is:

$$P_{CLK} = \frac{1}{2} \cdot \frac{4}{3} \cdot NC_G V_{DD}^2 F_{LO} + \frac{1}{2} \cdot \frac{4}{3} \cdot NMC_G V_{DD}^2 F_{IF}$$
$$= C_G V_{DD}^2 \cdot \left(\frac{2}{3} N F_{LO} + \frac{2}{3} N M F_{IF}\right)$$
(26)

where one set of N-phase mixers and N/2 sets of M-phase mixers are used for the proposed case. Equating (25) and (26) yields $F_{IF} = F_{LO}/M$. For N, M = 8 and $F_{LO} = 700$ MHz, the proposed case has a smaller dynamic consumption when F_{IF} is less than 87.5MHz, indicating a carrier separation of 175MHz apart. If M increases further to 16, the proposed case has a smaller dynamic consumption when F_{IF} is less than 43.75MHz.

2) Designing for Different Numbers of Clock Phases:

a) Baseband TIAs: To the first order, an increased number of clock phases does not increase baseband power consumption or area. From (14), as N, M increases, the number of baseband branches increases, and the overall noise performance can be kept constant by scaling down the individual TIA op-amps and their feedback capacitors and scaling up their feedback resistance. This is because the noise adds in power, whereas the signal adds in voltage [6].

b) RF mixer switches: When the number of clock phases increases, designers can choose to keep the mixer-switch sizes the same or to reduce the mixer-switch size. In the latter case, the mixer-clock dynamic power stays constant to the first order since the total switch size remains the same. However, smaller mixer switches have larger R_{SW} , resulting in a higher out-of-band impedance and less out-of-band blocker filtering. To maintain good out-of-band filtering, the switches need to be kept the same size; however, as their number increases with

the number of clock phases, the mixer-clock dynamic power will increase and require stronger clock buffers.

III. MODULATING THE LNTA TRANSCONDUCTANCE IN AN LNTA-PASSIVE MIXER RECEIVER BRANCH

A. Principle of Operation

Frequency translations in high-performance, current-mode receivers [2], [23] are usually realized by converting the RF voltage to current with LNTAs and then translating the RF information to baseband with passive mixers in the current domain. If the LNTA transconductance is periodically modulated, another frequency translation can be realized during the RF voltage-to-current conversion. In Fig. 7a, we introduce two quadrature-modulated LNTA branches (LBs), where each branch is composed of an *M*-phase-modulated LNTA and *N*-phase, current-mode mixers, followed by baseband TIAs and two harmonic recombination circuits. In practice, to simplify clock generation, *N*, *M* are integers greater than two and are typically powers of two (e.g., 8, 16, etc).

The two modulated LNTAs have sinusoidally-varying transconductances, $G_{m,I}(t)$ and $G_{m,Q}(t)$ in Fig. 7b, in quadrature at F_{IF} . They operate as switched- G_m mixers to translate $V_{RF}(\omega)$ at $(F_{LO}\pm F_{IF})$ to $I_{RF,I}(\omega)$ and $I_{RF,Q}(\omega)$ at F_{LO} , which are then translated to baseband with passive mixers driven by the same N-phase, non-overlapping clocks at F_{LO} . These baseband currents are converted to voltages with TIAs and are further harmonically re-combined to form four baseband signals, $V_{BB0}(\omega)$ to $V_{BB3}(\omega)$, while rejecting higher-order F_{LO} harmonics. The I/Q components from both RF carriers can be simply separated from these four baseband signals using addition and subtraction circuits (see also Section II-A).

B. Conversion Gain

The transconductance conversion gain of the modulated LNTAs, $G_{m,EQ}$, is defined as the ratio of $I_{RF,I}(\omega)$ at F_{LO} to $V_{RF}(\omega)$ at $(F_{LO} \pm F_{IF})$ and is the fundamental Fourier series coefficient of $G_{m,I}(t)$:

$$G_{m,EQ} \equiv \frac{I_{RF,I}}{V_{RF}} = \frac{1}{2} \cdot G_{m,pk} \cdot \operatorname{sinc}(\pi/M)$$
 (27)

where M is the number of the LNTA modulation phases, and $G_{m,pk}$ is the peak LNTA transconductance. To derive closed-form expressions for gain and noise performance, we assume that both $G_{m,I}(t)$ and $G_{m,Q}(t)$ are the discrete-time approximations of the sinusoids with un-quantized transconductance. The impact of quantization will be discussed later. $I_{RF,I}(\omega)$ at F_{LO} is then translated and converted to the voltage $V_{BBO}(\omega)$ at baseband by the transimpedance conversion gain:

$$R_{EQ} \equiv \frac{V_{BB0}}{I_{RF,I}} = G_{MX,LO}R_{F,LB} \cdot \frac{N}{2}$$
$$= \frac{1}{2} \cdot R_{F,LB} \cdot \operatorname{sinc}(\pi/N)$$
(28)

where $R_{F,LB}$ is the TIA feedback resistance, and $G_{MX,LO} = (1/N)\operatorname{sinc}(\pi/N)$ is the mixer current conversion gain [16]. Here we also assume un-quantized, baseband weightings in the harmonic rejection circuits. After sideband separation, the conversion gain doubles and is:

$$CG'_{LB,N-M} \equiv \frac{V_{BB,I-1}}{V_{RF}} = G_{m,EQ}R_{EQ} \cdot 2$$
$$= \frac{1}{2} \cdot G_{m,pk}R_{F,LB} \cdot \operatorname{sinc}(\pi/N) \cdot \operatorname{sinc}(\pi/M). \quad (29)$$

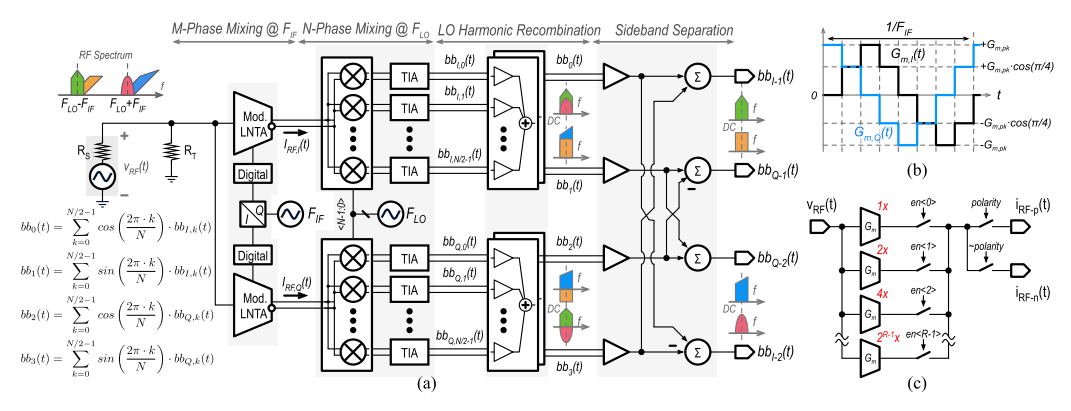


Fig. 7. (a) Block diagram of the quadrature-modulated LNTA branches with R_T for broadband input termination that can be replaced by a mixer-first branch (Section II); (b) Eight-phase example of sinusoidally time-varying transconductances; (c) Behavioral model of the modulated LNTAs in a single-ended-differential realization.

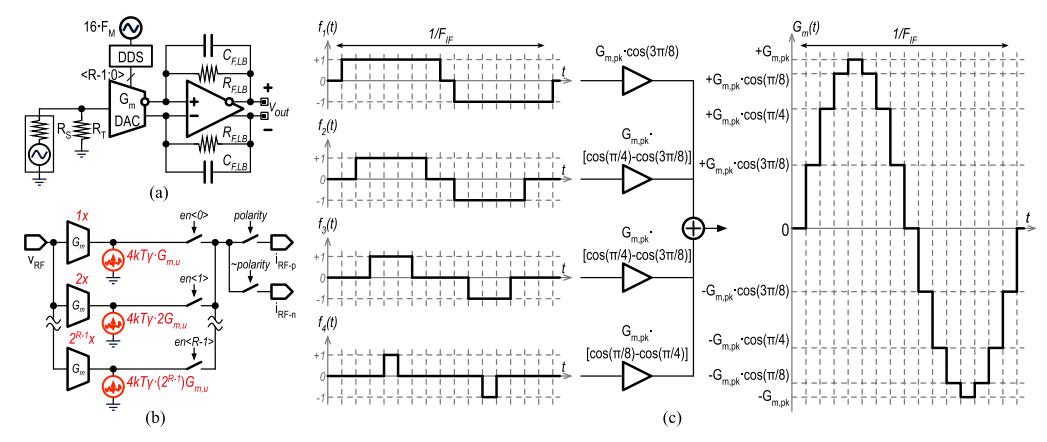


Fig. 8. (a) Schematic of the modulated LNTA directly followed by a baseband TIA; (b) Schematic of the modulated LNTA with noise sources for each cells; (c) Decomposition of a 16-phase modulated transconductance into four {-1,0,1} component waveforms.

As *N*, *M* increase, both sinc factors approach unity, and there will be less noise folding from higher-order harmonics and better harmonic suppression across the RF spectrum. If needed, a fully differential realization can be used to suppress common-mode interferences.

C. Noise

The LNTA branch does not provide impedance matching. However, this is required in practice and is done with another circuit (see also Section II-B). For the analysis of the LNTA branch, we model the impedance matching with a resistor R_T (Fig. 7a) that is equal to R_S for broadband matching. In a well-designed current-mode receiver, the LNTAs have a high output impedance; R_S , R_T , and the modulated LNTAs are the significant noise sources, while the noise from passive mixers, TIA feedback resistors, and TIA op-amps do not significantly contribute to the overall noise [17].

1) Noise From R_S and R_T : These noise sources share the same noise transfer function to the branch output; the noise contribution for R_S is:

$$\frac{\overline{v_{no,R_S}^2}}{\Delta f} = \frac{\overline{v_{n,R_S}^2}}{\Delta f} \cdot \left(\frac{CG'_{LB,N-M}}{2}\right)^2 \cdot \frac{2}{\operatorname{sinc}^2(\pi/N) \cdot \operatorname{sinc}^2(\pi/M)}$$
(30)

where $\overline{v_{n,R_S}^2}/\Delta f = 4kTR_S$ [18], and the factor of (1/2) stems from the fact that the noise process experiences a voltage division between R_S and R_T at the LNTA's input.

2) Noise From Modulated LNTAs: To understand the noise of modulated LNTAs in the overall signal branch, let us first consider the circuit in Fig. 8a, where the modulated LNTA is directly followed by a baseband TIA. It down-converts the signals at F_{IF} to baseband, while rejecting other higher-order F_{IF} clock harmonics. We model the noise of each unit cell as a shunt noise current source at the cell output (Fig. 8b) [18]. If a unit cell is used during LNTA modulation, its noise current appears at the TIA virtual ground and develop a noise voltage at the TIA output. Otherwise, if the cell is not used during modulation, it does not contribute noise.

Since the noise of each unit cell is un-correlated, we can then re-organize these unit cells; their equivalent, noise power spectral densities (PSDs) can be calculated from the sum of the individual noise PSDs. Thanks to the sinusoidal symmetry, we can decompose $G_{m,I}(t)$ into four components, $f_1(t)$ to $f_4(t)$ in Fig. 8c, with corresponding sinusoidal weights, compute the noise contribution of each component, and sum these contributions. Using the Parseval's theorem, the noise PSD can be derived from the integral of the square of a time-domain function over its period. The noise contribution at TIA output due to $f_1(t)$ is:

$$\frac{\overline{v_{n,f_1}^2}}{\Delta f} = 4kT\gamma G_{m,pk} \cos(\frac{3\pi}{8}) \cdot \frac{1}{T_{IF}} \int_0^{T_{IF}} |f_1(t)|^2 dt \cdot R_{F,LB}^2$$

$$= 4kT\gamma G_{m,pk} \cos(\frac{3\pi}{8}) \cdot \frac{7}{8} \cdot R_{F,LB}^2. \tag{32}$$

Similarly, the contributions of the other components can be computed; all four contributions can be summed to find the total noise PSD:

$$\frac{\overline{v_{n,G_m}^2}}{\Delta f} = \sum_{k=1}^4 \frac{\overline{v_{n,f_k}^2}}{\Delta f} = 4kT\gamma G_{m,pk} \cdot R_{F,LB}^2
\cdot \frac{1}{8} \left[1 + 2\cos(\frac{\pi}{8}) + 2\cos(\frac{\pi}{4}) + 2\cos(\frac{3\pi}{8}) \right]. \quad (33)$$

This expression includes the noise converted not only from the fundamental clock frequency at F_{IF} , but also from higher-order clock harmonics (e.g., 15^{th} and 17^{th} F_{IF} harmonics). This 16-phase result can be generalized to an M-phase modulated LNTA by decomposing its transconductance waveform into M/4 components and summing their contributions. For convenience, we refer this summed noise to the TIA input as:

$$\frac{\overline{i_{n,G_m}^2}}{\Delta f} = 4kT\gamma G_{m,pk} \cdot \frac{2}{M} \sum_{k=0}^{M/2-1} |\cos(\frac{2\pi}{M}k)|.$$
 (34)

Getting back to the overall signal branch in Fig. 7, the quadrature-modulated LNTAs are followed by N-phase passive mixers, baseband TIAs, and harmonic-recombining circuits. Extra noise will be down-converted from higher-order F_{LO} harmonics. In terms of noise process, the signal branch down-converts the noise from $(nF_{LO} + mF_{IF})$ to baseband, where $n = k_1 \ N \pm 1$, $m = k_2 \ M \pm 1$, and $k_1, k_2 \in \mathbb{Z}$. The resulting total noise at $V_{BB,I-1}$ in Fig. 7a is then:

$$\frac{\overline{v_{no,G_m}^2}}{\Delta f} = 2 \cdot \frac{\overline{i_{n,G_m}^2}}{\Delta f} \cdot R_{EQ}^2 \cdot \frac{2}{\operatorname{sinc}^2(\pi/N)}$$
(35)

where the factor of '2' is due to the fact that two modulated LNTAs are used. Substituting (34) and (28) into (35), we obtain:

$$\frac{\overline{v_{no,G_m}^2}}{\Delta f} = \frac{\overline{v_{n,G_{m,pk}}^2}}{\Delta f} \cdot (CG'_{LB,N-M})^2 \cdot \frac{4}{M} \sum_{k=0}^{M/2-1} |\cos(\frac{2\pi}{M}k)| \cdot \frac{2}{\sin^2(\pi/N) \cdot \sin^2(\pi/M)}$$
(36)

where $\overline{v_{n,G_{m,pk}}^2}/\Delta f = 4kT\gamma/G_{m,pk}$.

3) The Noise Factor: of the quadrature-modulated LNTA branches, $F'_{LB,N-M}$, can now be derived and is given in (31), as shown at the bottom of the page. If 8-phase-modulated LNTAs are used with 8-phase HR down-conversion circuits (i.e., N = M = 8), (31) reduces to:

$$F'_{LB,8-8} = \frac{1}{\operatorname{sinc}^4(\pi/8)} \cdot \left\{ 2 + \frac{2\gamma}{G_{m,pk}R_S} \cdot \left[1 + 2\cos(\frac{\pi}{4}) \right] \right\}. \tag{37}$$

Implications of these expressions will be discussed later and verified with simulation results.

D. Harmonic Rejection

The previous parts assume that the modulated LNTAs produce un-quantized transconductance, and that the harmonic recombination networks apply un-quantized weights to $bb_{I,i}(t)$ and $bb_{Q,i}(t)$. In practice, both weights are realized in a quantized manner. For modulated LNTAs, quantization errors result in undesired harmonic responses at higher-order F_{IF} harmonics. The harmonic rejection ratio (HRR) is the ratio of transconductance conversion gain at F_{IF} to the transconductance conversion gain at the i^{th} harmonic:

$$HRR_{i} \equiv \left| \frac{G_{m,EQ}}{G_{m,i}} \right| = \left| \frac{\frac{1}{T_{IF}} \int_{0}^{T_{IF}} G_{m,I}(t) \exp(1 \cdot j\omega_{IF}t) dt}{\frac{1}{T_{IF}} \int_{0}^{T_{IF}} G_{m,I}(t) \exp(i \cdot j\omega_{IF}t) dt} \right|.$$
(38)

For M = 8, (38) reduces to:

$$HRR_i = \left| \frac{\sin(\pi/8)}{\sin(i\pi/8)} \right| \cdot \left| \frac{1 + 2\rho_{IF} \cdot \cos(\pi/4)}{1 + 2\rho_{IF} \cdot \cos(i\pi/4)} \right|$$
 (39)

where ρ_{IF} is the ratio of the mid-level transconductance to the peak LNTA transconductance and should be $\cos(\pi/4)$, ideally. Due to quantization errors, it will deviate from this ideal value, resulting in a finite HRR and undesired signals around the F_{IF} clock harmonics being down-converted on top of the desired signals. For 4-bit resolution, the modulated LNTAs offer 36.7dB HRR₃ and 41.1dB HRR₅. Once improved to 5-bit resolution, the LNTAs now provide 56.7dB HRR₃ and 61.1dB HRR₅. Using a finer resolution or a larger M will lead to a higher HRR. Similarly, the HRR for M-phase-modulated LNTAs is:

$$HRR_{i} = \left| \frac{\operatorname{sinc}(\pi/M)}{\operatorname{sinc}(i\pi/M)} \right| \cdot \frac{\sum_{k=0}^{M/2-1} |\rho_{IF,k} \cdot \cos(\frac{2\pi}{M}k)|}{\sum_{k=0}^{M/2-1} |\rho_{IF,k} \cdot \cos(i\frac{2\pi}{M}k)|}$$
(40)

where $\rho_{IF,k}$ should be $\cos(2\pi k/M)$, ideally. For the whole signal branch, harmonic rejection happens in both the F_{LO} and the F_{IF} clock domains. To the first order, its HRR can be obtained by multiplying two HRR expressions. For N=M=8, it is:

$$HRR_{n,m} = \left| \frac{\sin(\pi/8)}{\sin(m\pi/8)} \cdot \frac{1 + 2\rho_{IF} \cdot \cos(\pi/4)}{1 + 2\rho_{IF} \cdot \cos(m\pi/4)} \right| \cdot \left| \frac{\sin(\pi/8)}{\sin(n\pi/8)} \cdot \frac{1 + 2\rho_{LO} \cdot \cos(\pi/4)}{1 + 2\rho_{LO} \cdot \cos(\pi/4)} \right|$$
(41)

where ρ_{LO} is the ratio of the baseband weight used in the harmonic recombination for the F_{LO} clock; n and m are the harmonic orders for the F_{LO} and the F_{IF} clocks, respectively. Ideally, both ρ_{LO} and ρ_{IF} should be $\cos(\pi/4)$. Note that (41) reduces to (22) when $n=k_1$ $N\pm 1$, $m=k_2$ $M\pm 1$, and $k_1,k_2\in\mathbb{Z}$. This is because the LNTA branches also employ the switching circuits for frequency translations and, thereby, face the same challenges from harmonic folding.

$$F'_{LB,N-M} = \frac{1}{\operatorname{sinc}^{2}(\pi/N) \cdot \operatorname{sinc}^{2}(\pi/M)} \cdot \left[2 + \frac{4\gamma}{G_{m,pk}R_{S}} \cdot \frac{4}{M} \sum_{k=0}^{M/2-1} \left| \cos(\frac{2\pi}{M} \cdot k) \right| \right]$$
(31)

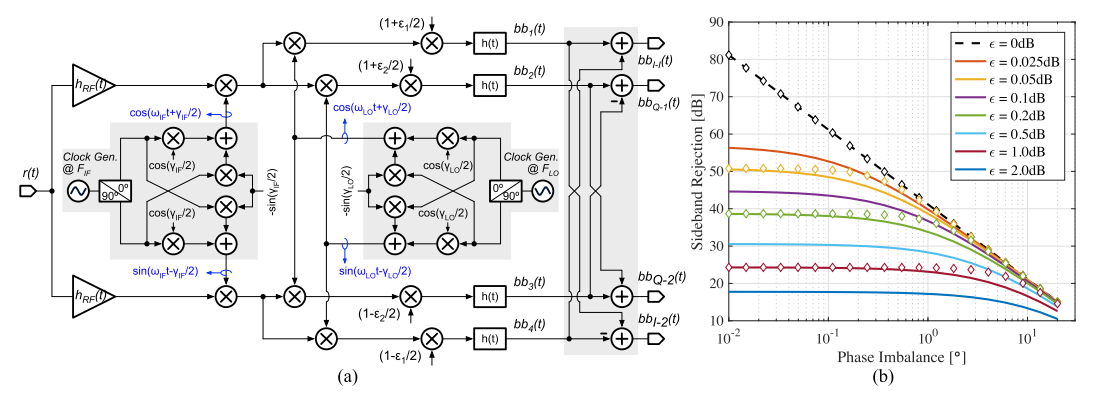


Fig. 9. (a) Model to study the effects of gain and phase imbalances on sideband rejection in the modulated LNTA branches. (b) Analytical (–) and simulated (\diamond) rejection versus phase imbalances for varying gain imbalances.

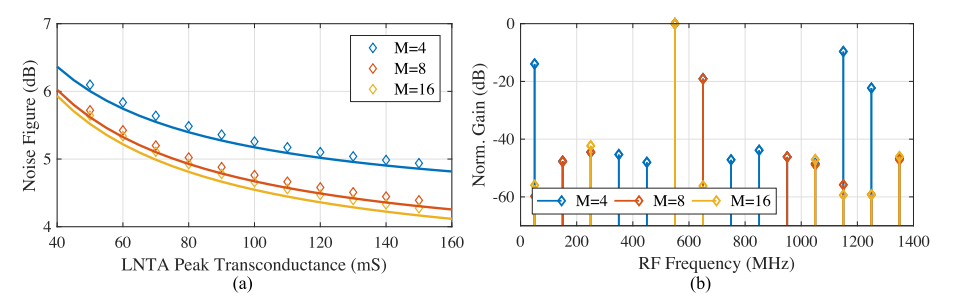


Fig. 10. (a) Analytical (–) and simulated (\diamond) NFs versus $G_{m,pk}$ in a single-ended-differential LNTA branch using N=8 but different M. (b) Simulated spurious responses for reception of a signal at 550MHz using N=8, $F_{LO}=700$ MHz and $F_{IF}=150$ MHz but different M.

E. Sideband Separation

So far, clocks have been assumed to be ideal with no phase or gain mismatches, and the analog circuits have been assumed to be perfectly phase and gain matched. In practice, non-idealities will occur, and as a result, the low-band outputs will contain signal components that are down-converted from the higher RF carrier and vice versa.

The model in Fig. 9a is used to study the effects of phase and gain imbalances on the sideband rejection, where γ_{LO} and γ_{IF} are the phase imbalances for the F_{LO} and F_{IF} clock domains, respectively [24], and ϵ_1 and ϵ_2 are the amplitude imbalances due to the analog circuitry. For the quadrature-modulated LNTA branches, the F_{IF} clocks are running at a much lower rate, compared to the F_{LO} clock rate. Thus, we can neglect the phase imbalances due to the F_{IF} clocks by assuming γ_{IF} is zero. The sideband rejection is defined as the ratio of the down-converted signal power from the desired RF carrier to the down-converted signal power from the undesired RF carrier:

$$SBR = \frac{1 + \cos\left[\gamma_{LO} + 2 \cdot \operatorname{atan}(\epsilon_1/2)\right]}{1 - \cos\left[\gamma_{LO} - 2 \cdot \operatorname{atan}(\epsilon_1/2)\right]}.$$
 (42)

Fig. 9b plots the analytical and simulated rejection versus phase imbalances with different levels of gain imbalances. The analytical results agree well with the simulated results. To demodulate an uncoded QAM-1024 modulated signal⁶ with a bit error ratio of 10^{-6} , a minimum signal-to-noise ratio (SNR) of 39.0dB is needed [25], meaning the phase imbalance needs to be 1° , while the gain imbalances should

stay below 0.2dB. Note that the sideband rejection of the double-layer mixer-first branch will share the same expression since its mathematical model is the same as the model in Fig.9a.

F. Simulations and Design Considerations

Fig. 10a shows the analytical and simulated NFs as a function of $G_{m,pk}$ for N=8 but using different M in a single-ended-differential realization. The simulation uses $R_S=R_T=50\Omega$, $\gamma=2/3$, and 8-bit modulated LNTAs. Both analytical and simulated results agree within 0.1dB. The noise performance gets improved significantly from M=4 to M=8, thanks to less noise being folded from the F_{IF} clock domain, but not that much from M=8 to M=16. Ultimately, the effect of noise folding can be neglected, and the noise performance will be dominated by the noise from the fundamental tone at F_{IF} . As M becomes very large, the noise factor in (31) approaches:

$$\lim_{M \to \infty} F'_{LB,N-M} = \frac{1}{\operatorname{sinc}^2(\pi/N)} \cdot \left(2 + \frac{4\gamma}{G_{m,pk}R_S} \cdot \frac{4}{\pi}\right). \quad (43)$$

Fig. 10b shows the simulated spurious responses for N=8 but using different M to illustrate how selection of M affects the spurious response of the signal branch. The simulations use $F_{LO}=700 \mathrm{MHz}$ and $F_{IF}=150 \mathrm{MHz}$; the signal branch is configured to receive the lower RF carrier at $(F_{LO}-F_{IF})=550 \mathrm{MHz}$. Eq. (22) can be used to calculate the HFRR. The responses at 650 MHz, 1150 MHz and 1250 MHz are caused by the harmonic folding from $(F_{LO}-9~F_{IF})$, $(F_{LO}+3~F_{IF})$ and $(F_{LO}-13~F_{IF})$, respectively. The calculated HFRRs are 19.1dB, 9.5dB, and 22.3dB, respectively; they agree fairly well with the simulated results. As M increases from 4 to 8, the responses at 1150 MHz and 1250 MHz are suppressed. The response at 650 MHz still exists, because 8-phase clocking

⁶We assume that the received power levels for both carriers are the same. In practice, wireless standards [3] often require the power levels of the assigned RF carriers to stay within a small range to maintain the same SNR for the same modulation scheme to double the throughput.

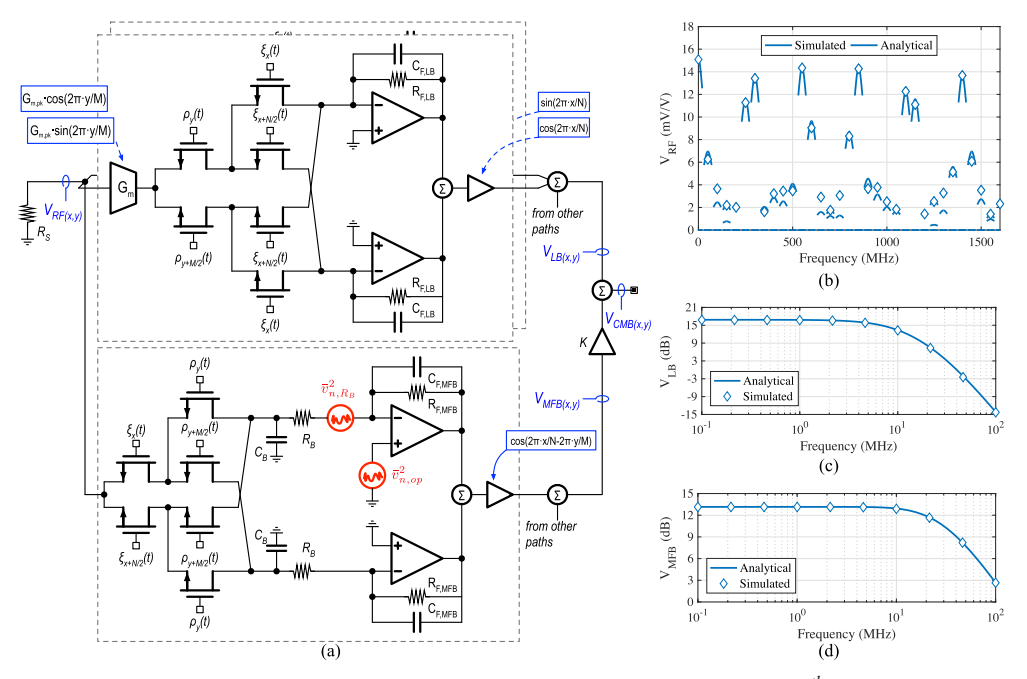


Fig. 11. Analysis of the double-conversion, noise-cancelling receiver: (a) Simplified schematic for the $(x, y)^{th}$ path; analytical and simulated responses at the RF input (b), the quadrature-modulated LNTA output (c), and the double-layer, mixer-first branch output (d) using N = M = 8, $F_{LO} = 700$ MHz, $F_{IF} = 150$ MHz, $F_{S} = 50\Omega$, $F_{SW} = 10\Omega$, $F_{SW} = 1.06$ k $F_$

systems simply cannot suppress the 9^{th} order harmonic. When M increases to 16, this response gets additionally suppressed; the spurious responses are better than 40dB across the interested RF range. Therefore, it is desirable in practice to have a large number of LNTA modulation phases for better spurious response profiles.

1) Comparison to Standard LNTA Branches: For standard LNTA branches [2] driven by N-phase, non-overlapping clocks at F_{LO} , whose LNTA provides a fixed transconductance, its NF can be calculated as 4.3dB for N=8, $\gamma=2/3$ and $G_{m,pk}=90$ mS. In our case, from (31), the calculated NFs are 5.2dB, 4.7dB, 4.6dB for M=4, 8, and 16, respectively. When M gets very large, its NF can be calculated as 4.6dB, indicating a NF penalty of 0.3dB compared to that of standard LNTA branches.

IV. COMBINING DOUBLE-LAYER MIXER-FIRST BRANCH AND QUADRATURE-MODULATED LNTA BRANCH INTO A DOUBLE-CONVERSION, NOISE-CANCELLING RECEIVER

In FTNC receivers [17], the noise of R_{SW} , R_B , and baseband op-amps in the mixer-first branch not only propagates to the mixer-first branch outputs (see Section II-D), but also is up-converted to the RF input and appear at the LNTA branch outputs. These output noise contributions are anti-correlated and can be cancelled by combining the outputs of both signal branches with appropriate gain coefficients, while the signal components are correlated and add up constructively. In this section, the double-layer mixer-first branch and the quadrature-modulated LNTA branches are combined to form the proposed double-conversion, noise-cancelling receiver that inherits the input matching properties of the double-layer mixer-first branch while having much better sensitivity.

A. Noise-Cancelling (NC) Condition

To derive the NC condition, two observations can be made. The noise of R_B and the baseband op-amps from the

mixer-first branch are orthogonal and un-correlated between different signal paths (see also Section II-D), allowing us to study one path and then generalize its result to all other paths. Fig. 11a will be used to study the NC condition of the $(x, y)^{th}$ path, where K is the coefficient to adjust the relative gain difference between two branch outputs $V_{MFB(x,y)}$ and $V_{LB(x,y)}$.

Another observation is that random noise can be represented as a summation of a great number of equally-spaced sinusoidal tones, whose amplitudes are independent random variables distributed normally about zero, and whose phases are also independent random variables and distributed uniformly from 0 to 2π [26]. Therefore, a noise source can then be replaced with an equivalent AC source, and its AC response within the system can be studied. Now we replace its noise source of the R_B resistor in the $(x, y)^{th}$ path with $V_{n,R_B}(\omega)$. Its transfer function to $V_{MFB(x,y)}$ is:

$$\frac{V_{MFB(x,y)}(\omega)}{V_{n,R_B}(\omega)} = \frac{R_{F,MFB}}{R_1 + R_B} \cdot \frac{1}{1 + j\omega R_{F,MFB} C_{F,MFB}} \\
\cdot \frac{1 + j\omega R_1 C_B}{1 + j\omega (R_1 \| R_B) C_B} \cdot \cos\left(\frac{2\pi}{N} x - \frac{2\pi}{M} y\right) (46)$$

where the cos factor stems from harmonic recombination and sideband separation. The transfer function to $V_{BB(x,y)}$ path is:

$$\frac{V_{BB(x,y)}(\omega)}{V_{n,R_B}(\omega)} = \frac{R_1}{R_1 + R_B} \cdot \frac{1}{1 + j\omega(R_1 \parallel R_B)C_B}$$
(47)

where $R_1 = (R_S + 2R_{SW}) \cdot (NM/2)$ (see Section II-D). From time-domain, this voltage will appear at RF input during two time windows, $\xi_x(t) \cdot \rho_y(t)$ and $\xi_{x+N/2}(t) \cdot \rho_{y+M/2}(t)$. From frequency-domain, it means that $V_{BB(x,y)}$ will be translated to $(pF_{LO} + qF_{IF})$ as (44), as shown at the bottom of the next page, where (p+q) is even. This RF voltage is then seen by the modulated LNTA branches. Since we are only interested in the baseband components, the derivations can be greatly simplified

with $V_{LB(x,y)}$ given in (45), as shown at the bottom of the page. If we further restrict our attention to the frequency components well within the channel (i.e., $\Delta \omega \approx 0$), $V_{CMB(x,y)}(\omega)$ becomes:

$$\frac{V_{CMB(x,y)}(\Delta\omega)}{V_{n,R_B}(\Delta\omega)} = \frac{G_{m,pk}R_SR_{F,LB} + K \cdot R_{F,MFB}}{R_1 + R_B} \cdot \cos\left(\frac{2\pi}{N}x - \frac{2\pi}{M}y\right) \quad (48)$$

where the NC condition can be found by setting (48) to zero as:

$$K'_{NC} = -1 \cdot G_{m,pk} R_S \cdot \frac{R_{F,LB}}{R_{F,MFB}}.$$
 (49)

Figs. 11b, 11c and 11d shows the analytical and the simulated responses at $V_{RF(x,y)}$, $V_{LB(x,y)}$ and $V_{MFB(x,y)}$, respectively. Both results agree fairly well with each other. Following the same logic, we replace the noise source of the baseband op-amp with an AC source $V_{n,op}(\omega)$ and find its transfer function to $V_{CMB(x,y)}$ as:

$$\frac{V_{CMB,OP(x,y)}(\Delta\omega)}{V_{n,op}(\Delta\omega)}$$

$$= \frac{1}{R_1 + R_B} \cdot \cos\left(\frac{2\pi}{N}x - \frac{2\pi}{M}y\right)$$

$$\cdot \left[G_{m,pk}R_SR_{F,LB} + K \cdot \left(R_1 + R_B + R_{F,MFB}\right)\right]. \quad (50)$$

B. Conversion Gain Under NC Condition

While the noise of R_B and baseband op-amps is anti-correlated at $V_{LB(x,y)}$ and $V_{MFB(x,y)}$, the down-converted signals are actually correlated at these two nodes. Under the NC condition, the desired signals add up constructively; the receiver conversion gain becomes:

$$CG'_{RX,N-M} \equiv CG'_{LB,N-M} - K'_{NC,RB} \cdot CG'_{MFB,N-M}$$

= $CG'_{LB,N-M} \cdot \left(1 + \frac{R_S}{2R_{SW} + 2\eta R_B}\right)$ (51)

where, as expected, the expression is a function of R_B . When the input impedance is matched (i.e., $2R_{SW} + 2\eta R_B = R_S$), the receiver conversion gain is twice the conversion gain of the modulated LNTA branches.

C. Noise Under NC Condition

1) Noise From R_S and R_{SW} : Behaving similarly as signals, the noise of R_S propagates to the outputs of the two branches creating correlated components. Its noise contribution at V_{CMB} is:

$$\frac{1}{\sqrt{2}} \cdot \cos\left(\frac{2\pi}{N}x - \frac{2\pi}{M}y\right) \quad (48) \quad \frac{\frac{1}{\sqrt{2}}}{\Delta f} = \frac{\frac{1}{\sqrt{2}}}{\Delta f} \cdot \frac{2}{\sin^2(\pi/M) \cdot \sin^2(\pi/N)}$$
bund by setting (48) to zero
$$\cdot \left[\frac{2R_{SW} + 2\eta R_B}{R_S + 2R_{SW} + 2\eta R_B} \cdot \left(CG'_{LB,N-M} - K \cdot CG'_{MFB,N-M}\right)\right]^2 \quad (52)$$

where the multiplication factor inside the bracket is the voltage division ratio between R_S and R_{in} . Under the NC condition, (52) reduces to:

$$\frac{\overline{v_{no,R_S}^2}}{\Delta f} = \frac{\overline{v_{n,R_S}^2}}{\Delta f} \cdot CG_{LB,N-M}^{2} \cdot \frac{2}{\operatorname{sinc}^2(\pi/M) \cdot \operatorname{sinc}^2(\pi/N)}.$$
(53)

The noise of R_S is now not a function of input matching anymore. Qualitatively, with large R_{in} , the noise at the LNTA branch outputs increases, whereas the noise at the mixer-first branches decreases, and vice versa for the case of small R_{in} . For both scenarios, the output noise due to R_S stays constant. For the noise of R_{SW} , it creates anti-correlated components at two branch outputs; under the NC condition, the noise of R_{SW} gets cancelled, meaning that $\overline{v_{no,R_{SW}}^2}/\Delta f=0$.

2) Noise From R_B and Baseband Op-Amps: Section IV-A

derives the noise transfer functions of the $(x, y)^{th}$ path to $V_{CMB(x,y)}$ for both R_B and the baseband op-amps. Therefore, the output noise due to R_B can be derived by summing their contributions from all the paths as:

$$\frac{\overline{v_{no,R_B}^2}}{\Delta f} = \frac{\overline{v_{n,R_B}^2}}{\Delta f} \cdot \frac{NM}{4} \cdot \left(\frac{G_{m,pk}R_SR_{F,LB} + K \cdot R_{F,MFB}}{R_1 + R_B}\right)^2 \tag{55}$$

where its value reduces to zero under the NC condition. Similarly, the output noise of the baseband op-amps, under the NC condition, can be derived and simplified as:

$$\frac{\overline{v_{no,op}^2}}{\Delta f} = \frac{\overline{v_{n,op}^2}}{\Delta f} \cdot \frac{NM}{2} \cdot (CG'_{LB,N-M} \cdot \frac{R_S}{R_{MFB}})^2 \cdot \frac{2}{\sin^2(\pi/N) \cdot \sin^2(\pi/M)}.$$
(56)

$$V_{RF(x,y)}(\omega) = \mathcal{F}\langle\left\{\frac{R_{S}}{R_{S} + 2R_{SW}} \cdot \left[\xi_{x}(t) \cdot \rho_{y}(t) + \xi_{x+N/2}(t) \cdot \rho_{y+M/2}(t)\right]\right\} \cdot v_{BB}(t)\rangle$$

$$= \frac{R_{S}}{R_{S} + 2R_{SW}} \cdot \sum_{p=-\infty}^{+\infty} \sum_{q=-\infty}^{+\infty} \alpha_{p} \beta_{q} \cdot \left\{1 + \exp[-j(p+q)\pi]\right\} \cdot \exp(-jxp\frac{2\pi}{N}) \cdot \exp(-jyq\frac{2\pi}{M}) \cdot V_{BB}\left[\omega - (p\omega_{LO} + q\omega_{IF})\right]$$

$$V_{LB(x,y)}(\omega) = V_{BB(x,y)}(\omega) \cdot \frac{R_{S}}{R_{S} + 2R_{SW}} \cdot \frac{G_{m,pk}R_{F,LB}}{1 + j\omega R_{F,LB}C_{F,LB}} \cdot \cos\left(\frac{2\pi}{N}x - \frac{2\pi}{M}y\right) \cdot \sum_{p=-\infty}^{+\infty} \sum_{q=-\infty}^{+\infty} |\alpha_{p}|^{2} |\beta_{q}|^{2} \cdot \left\{1 + \exp[-j(p+q)\pi]\right\}^{2}$$

$$= V_{n,R_{B}}(\omega) \cdot G_{m,pk}R_{S} \cdot \frac{R_{F,LB}}{R_{1} + R_{B}} \cdot \frac{1}{1 + j\omega(R_{1} \parallel R_{B})C_{B}} \cdot \frac{1}{1 + j\omega R_{F,LB}C_{F,LB}} \cdot \cos\left(\frac{2\pi}{N}x - \frac{2\pi}{M}y\right)$$

$$(45)$$

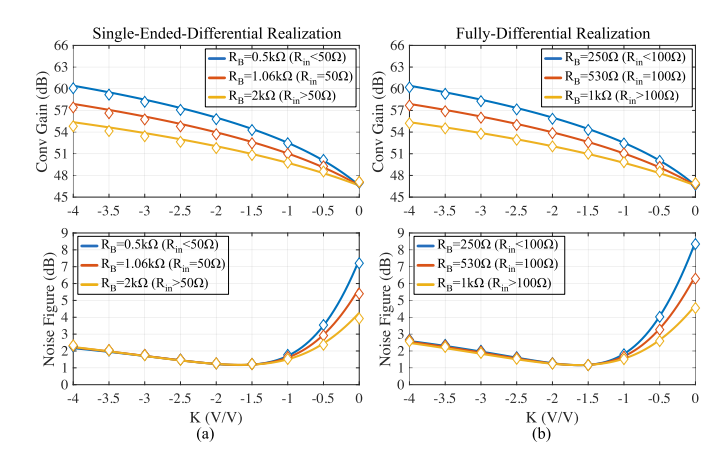


Fig. 12. Analytical and simulated gain and NFs for the double-conversion receiver as a function of K with different R_B values using N=M=8, $F_{LO}=700 \mathrm{MHz}, F_{IF}=150 \mathrm{MHz}, R_{SW}=10 \Omega, G_{m,pk}=90 \mathrm{mS}, G_{m,op}=625 \mathrm{uS}, R_{F,LB}=5 \mathrm{k}\Omega,$ and $R_{F,MFB}=15 \mathrm{k}\Omega$: (a) Single-ended-differential realization with $R_S=100 \Omega$.

We can now compare it with the noise due to the modulated LNTAs in (36). Using the parameters in Fig. 11, (36) can be calculated as 14.2fV²/Hz, whereas (56) as 0.6fV²/Hz. The noise due to the baseband op-amps under the NC condition is then much smaller than the noise due to the modulated LNTAs and can be ignored.

3) Noise Factor of the Double-Conversion Receiver: Since the noise due to the modulated LNTAs stays the same, the noise factor of the complete receiver, $F'_{RX,N-M}$, is derived in (54), as shown at the bottom of the page, where the third term stems from the noise due to baseband op-amps and is much smaller than the noise due to the modulated LNTAs. For N = M = 8, (54) reduces to:

$$F'_{RX,8-8} \approx \frac{1}{\operatorname{sinc}^4(\pi/8)} \cdot \left\{ 1 + \frac{\gamma}{G_{m,pk} R_S} \cdot \left[\frac{1}{2} + \cos\left(\frac{\pi}{4}\right) \right] \right\}$$
 (57)

Implications of this expression will be discussed and verified with simulation results in Section IV-D.

D. Simulations and Design Considerations

Fig. 12 shows the comparison of the analytical and simulated profiles for conversion gain and NF under different input matching conditions for both the single-ended-differential realization and the fully-differential realization. Both the analytical and simulated results agree well with each other. Interestingly, different matching conditions yield the same minimum NF of 1.2dB. This is because, under the NC condition, the output noise due to R_S is no longer a function of input matching or R_B . The noise due to R_B and R_{SW} in the mixer-first branch gets cancelled completely. The noise due to baseband op-amps get mostly cancelled; it is much smaller than the noise due to the modulated LNTAs and can be ignored. The receiver's noise performance is then mostly determined by the modulated LNTAs, whose noise stays the same regardless of matching

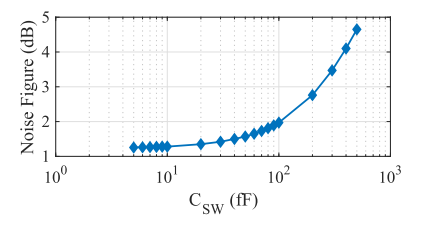


Fig. 13. Simulated receiver NF versus the mixer switch capacitance C_{SW} using the design parameters in Fig. 12.

conditions. Therefore, the total output noise stays constant regardless of matching conditions.

1) Comparison to Standard FTNC Receivers: For a FTNC receiver driven by N-phase, non-overlapping clocks at F_{LO} , its noise factor is derived in [17] as:

$$\widetilde{F}_{RX,N} \approx \frac{1}{\operatorname{sinc}^2(\pi/N)} \cdot \left(1 + \frac{\gamma}{G_{m,pk}R_S}\right).$$
 (58)

where the noise performance of the receiver is also dominated by the LNTA. For N=8, $R_S=50\Omega$, $G_{m,pk}=90\text{mS}$, the calculated NF is 0.8dB. With the same parameters, (54) can be calculated as 1.2dB for M=8 and 1.0dB for M=16. If M keeps increasing, (54) finally approaches:

$$\lim_{M \to \infty} F'_{RX,N-M} \approx \frac{1}{\operatorname{sinc}^2(\pi/N)} \cdot \left(1 + \frac{\gamma}{G_{m,pk}R_S} \cdot \frac{4}{\pi}\right) \tag{59}$$

where its NF can be calculated as 1.0dB, indicating a noise penalty of 0.2dB due to LNTA transconductance modulation. However, the standard FTNC receivers only receive one RF carrier at a time, whereas the double-conversion, noise-cancelling receiver can concurrently receive two carriers.

2) Design Considerations: In practice, parasitics exist and degrade the receiver's performance. For example, parasitic capacitance from the mixer switch devices (i.e., the junction capacitance between drain/source and substrate) and other loadings (e.g., ESD diodes and LNTA gates) reduces the RF bandwidth at V_{RF} and introduces additional but different phase shifts and attenuations to the up-converted, baseband termination noise at $(pF_{LO} + qF_{IF})$ (see Section IV-A). This noise then gets converted by the LNTA branches to baseband for noise cancellation. However, due to the different phase shifts and attenuations, the termination noise cannot be fully cancelled, resulting in degraded noise performance.

To study this effect, switch capacitance C_{SW} is additionally modelled into each of the mixer switch devices; the receiver's noise performance is simulated in Fig. 13. As C_{SW} increases, the simulated NF also increases. In fact, to maintain a good noise performance, all significant, higher-order intermodulation products at $(pF_{LO}+qF_{IF})$, e.g., up to 9^{th} clock harmonics for N=M=8, must be inside the RF bandwidth [17], such that the introduced phase shifts and attenuations are reduced. To mitigate this effect, advanced processes with reduced parasitics (e.g., SOI) can be used to improve the RF bandwidth at the receiver's input.

$$F'_{RX,N-M} = \frac{1}{\operatorname{sinc}^{2}(\pi/N) \cdot \operatorname{sinc}^{2}(\pi/M)} \cdot \left[1 + \frac{\gamma}{G_{m,pk}R_{S}} \cdot \frac{4}{M} \sum_{k=0}^{M/2-1} |\cos(\frac{2\pi}{M}k)| + \frac{\gamma}{G_{m,op}R_{S}} \cdot \frac{NM}{2} \cdot \left(\frac{R_{S}}{R_{F,MFB}}\right)^{2} \right]$$
(54)

V. CONCLUSION

We first explored the unique benefits of using double-layer passive mixing for concurrent tuned matching and reception at $(F_{LO} \pm F_{IF})$. For better receiver sensitivity, quadrature-modulated LNTA branches are added, where transconductance modulation is exploited to provide an additional frequency translation. By properly combining the outputs from both signal branches, the noise of R_{SW} , R_B , and the baseband op-amps from the mixer-first branch is cancelled. Mathematical expressions for RF input impedance, conversion gain, noise factor, and other metrics are provided to guide future designs and are verified with behavioral simulations.

ACKNOWLEDGMENT

The authors would like to thank Zhaowen Wang and Tanbir Haque from Columbia University for technical discussions and the reviewers for their valuable comments.

REFERENCES

- A. A. Abidi, "Direct-conversion radio transceivers for digital communications," *IEEE J. Solid-State Circuits*, vol. 30, no. 12, pp. 1399–1410, Dec. 1995.
- [2] D. Murphy et al., "A blocker-tolerant, noise-cancelling receiver suitable for wideband wireless applications," *IEEE J. Solid-State Circuits*, vol. 47, no. 12, pp. 2943–2963, Dec. 2012.
- [3] Evolved Universal Terrestrial Radio Access (E-UTRA); User Equipment (UE) Radio Transmission and Reception, document TS 36.101, 3GPP, 2017.
- [4] D. R. Pehlke and K. Walsh, "LTE-advanced pro RF front-end implementations to meet emerging carrier aggregation and DL MIMO requirements," *IEEE Commun. Mag.*, vol. 55, no. 4, pp. 134–141, Apr. 2017.
- [5] J. Zhu and P. R. Kinget, "Frequency-translational quadrature-hybrid receivers for very-low-noise, frequency-agile, scalable inter-band carrier aggregation," *IEEE J. Solid-State Circuits*, vol. 51, no. 12, pp. 3137–3151, Dec. 2016.
- [6] H. Wu, D. Murphy, and H. Darabi, "A harmonic-selective multi-band wireless receiver with digital harmonic rejection calibration," *IEEE J. Solid-State Circuits*, vol. 54, no. 3, pp. 796–807, Mar. 2019.
- [7] A. Agrawal and A. Natarajan, "An interferer-tolerant CMOS code-domain receiver based on N-path filters," *IEEE J. Solid-State Circuits*, vol. 53, no. 5, pp. 1387–1397, May 2018.
- [8] G. Han, T. Haque, M. Bajor, J. Wright, and P. R. Kinget, "A multi-branch receiver with modulated mixer clocks for concurrent dual-carrier reception and rapid compressive-sampling spectrum scanning," *IEEE J. Solid-State Circuits*, vol. 56, no. 1, pp. 235–253, Jan. 2021.
- [9] A. Elmaghraby, M. Hamouda, G. Fischer, R. Weigel, and T. Ussmueller, "A double bandpass N-path filter for LTE carrier aggregation receivers in 28 nm CMOS," in *Proc. WAMICON*, Jun. 2014, pp. 1–3.
- [10] R. Kasri, E. Klumperink, P. Cathelin, E. Tournier, and B. Nauta, "A digital sine-weighted switched-GM mixer for single-clock power-scalable parallel receivers," in *Proc. IEEE Custom Integr. Circuits Conf.* (CICC), Apr. 2017, pp. 1–4.
- [11] A. Mirzaei, H. Darabi, and D. Murphy, "Architectural evolution of integrated M-phase high-Q bandpass filters," *IEEE Trans. Circuits Syst. I, Reg. Papers*, vol. 59, no. 1, pp. 52–65, Aug. 2012.
- [12] G. Han, "High-performance reconfigurable RFIC architectures for concurrent signal reception," Ph.D. dissertation, Dept. Elect. Eng., Columbia Univ., New York, NY, USA, 2021.
- [13] C. Andrews and A. C. Molnar, "Implications of passive mixer transparency for impedance matching and noise figure in passive mixer-first receivers," *IEEE Trans. Circuits Syst. I, Reg. Papers*, vol. 57, no. 12, pp. 3092–3103, Dec. 2010.
- [14] D. Yang, C. Andrews, and A. Molnar, "Optimized design of N-phase passive mixer-first receivers in wideband operation," *IEEE Trans. Cir*cuits Syst. I, Reg. Papers, vol. 62, no. 11, pp. 2759–2770, Nov. 2015.
- [15] A. Ghaffari, E. A. M. Klumperink, M. C. M. Soer, and B. Nauta, "Tunable high-Q N-path band-pass filters: Modeling and verification," *IEEE J. Solid-State Circuits*, vol. 46, no. 5, pp. 998–1010, May 2011.
- [16] H. Darabi, Radio-Frequency Integrated Circuits and Systems, 1st ed. Cambridge, U.K.: Cambridge Univ. Press, 2015.

- [17] D. Murphy, A. Mirzaei, H. Darabi, M.-C.-F. Chang, and A. Abidi, "An LTV analysis of the frequency translational noise-cancelling receiver," *IEEE Trans. Circuits Syst. I, Reg. Papers*, vol. 61, no. 1, pp. 266–279, Jan. 2014.
- [18] B. Razavi, Design of Analog CMOS Integrated Circuits, 1st ed. New York, NY, USA: McGraw-Hill, 2000.
- [19] H. Darabi and A. A. Abidi, "Noise in RF-CMOS mixers: A simple physical model," *IEEE J. Solid-State Circuits*, vol. 35, no. 1, pp. 15–25, Jan. 2000.
- [20] M. Darvishi, R. van der Zee, E. A. M. Klumperink, and B. Nauta, "Widely tunable 4th order switched G_m-C band-pass filter based on N-path filters," *IEEE J. Solid-State Circuits*, vol. 47, no. 12, pp. 3105–3119, Nov. 2012.
- [21] Y. Xu, J. Zhu, and P. R. Kinget, "A blocker-tolerant RF front end with harmonic-rejecting *N*-path filter," *IEEE J. Solid-State Circuits*, vol. 53, no. 2, pp. 327–339, Feb. 2018.
- [22] Spectre Circuit Simulation Tool. Accessed: Dec. 2020. [Online]. Available: https://www.cadence.com
- [23] I. Fabiano, M. Sosio, A. Liscidini, and R. Castello, "SAW-less analog front-end receivers for TDD and FDD," *IEEE J. Solid-State Circuits*, vol. 48, no. 12, pp. 3067–3079, Dec. 2013.
- [24] B. Razavi, "Design considerations for direct-conversion receivers," *IEEE Trans. Circuits Syst. II, Analog Digit. Signal Process.*, vol. 44, no. 6, pp. 428–435, Jun. 1997.
- [25] J. Cioffi. Signal Processing and Detection. Stanford, CA, USA: Stanford Univ., 2014. [Online]. Available: http://web.stanford.edu/group/cioffi/doc/book/chap1.pdf
- [26] S. O. Rice, "Mathematical analysis of random noise," Bell Syst. Tech. J., vol. 23, no. 3, pp. 282–332, Jul. 1944.



Guoxiang Han (Member, IEEE) received the B.S. degree in electrical engineering from the Beijing Institute of Technology, Beijing, China, in 2015, and the M.S. degree in electrical engineering from Columbia University, New York, NY, USA, in 2016, where he is currently pursuing the Ph.D. degree with the Department of Electrical Engineering. His research interest includes reconfigurable receivers for concurrent reception.



Peter R. Kinget (Fellow, IEEE) received the Engineering degree in electrical and mechanical engineering and the Ph.D. degree in electrical engineering from Katholieke Universiteit Leuven, Belgium, in 1990 and 1996, respectively.

He has worked in industrial research and development at Bell Laboratories, Broadcom, Celight, and Multilink, before joining as a Faculty Member with the Department of Electrical Engineering, Columbia University, NY, USA, in 2002, where he is currently the Bernard J. Lechner Professor in electrical engi-

neering. From 2017 to 2020, he served as the Department Chair. He is also a consulting expert on patent litigation and a technical consultant to industry. His research interests include analog, RF, and power integrated circuits and the applications they enable in communications, sensing, and power management.